Indian Journal of Engineering & Materials Sciences
Vol. 33, April 2026, pp. 193-199
DOI: 10.56042/ijems.v33i02.23625

Investigating the effect of non-uniform ceramic dispersion on the mechanical properties of hybrid Al-Cu composite via powder metallurgy route

Venkatesh Sivakumar Meenatchi, Omprabba Kannan Chandramohan, Ramanaa Tharani & Venkatesan Muniyandi*

School of Mechanical Engineering, SASTRA Deemed University, Thanjavur 613 401, Tamil Nadu, India

Received: 10 September 2025; accepted: 28 January 2026

This study has used the powder metallurgy route to investigate the influence of varying ratios of SiO_2 and CrB_2 reinforcement on the mechanical properties of aluminium-copper alloy. Aluminium-copper alloys have been used in the fabrication of aircraft and automobile components. In the present work, SiO_2 has been synthesized by a sol-gel process, and UV-Vis and FTIR analyses have confirmed the quality of the synthesis. Varying ratios (0:1, 0.5:1, 1:1) of CrB_2 and SiO_2 have been mixed with Al+4wt% Cu, and the mixture undergoes cold compaction and sintering. The mechanical properties of the base metal alloy and hybrid composites have been compared. A maximum sintered density of 92.1% has been observed after reinforcement. Hardness values have consistently increased with increasing reinforcement amount. Adding 5 wt% of CrB_2 and SiO_2 has increased hardness by 52%, whereas compression strength has decreased by 34.4%. As the ceramic percentage has increased, compression strength has decreased, contrary to the reported trend. Inhomogeneously dispersed ceramic particles on a metal matrix and poor interfacial bonding have been attributed to this reduction. The results have inferred that the homogeneity of reinforcement distribution serves as a decisive factor in determining the ultimate mechanical properties of composites fabricated via powder metallurgy

Keywords: Ceramics, Composites, Hardness, Powder metallurgy, Sol-gel process

1 Introduction

The demand for high strength-to-weight ratio materials having lightweight properties is growing daily in the automotive sector[1-6]. Aluminium with low density (2.7 g/cm^3) and good corrosion resistance is a promising base material for such applications. However, its low hardness, yield strength, and wear resistance restrict the use in many demanding situations. To overcome these limitations, aluminum can be reinforced with hard particles such as carbides and oxides[7]. Particle-reinforced aluminum matrix composites exhibit enhanced performance characteristics and can retain their mechanical properties at high temperatures over standard aluminum alloys[8]. Traditional methods such as stir casting and squeeze casting routes at the liquid state and solid state manufacturing methods (friction stir welding, high energy ball milling, diffusion bonding) are generally used to fabricate Aluminum composites[9-12]. Previous studies found that aluminium-based composite fabricated by traditional casting methods has poor wettability because of the agglomeration of reinforcement particles, which leads to a depletion of mechanical properties. Aluminum powder metallurgy (P/M) is a cross-variable engine platform, which represents a reliable and economically viable manufacturing technology that can overcome the above-mentioned difficulties[13].

Al-Cu alloy, having light weight and high load-bearing capacity, was used to fabricate aircraft fittings and automotive components[14]. Among the alloy elements, copper has a good strengthening effect and high solubility within the Al matrix[15]. There are several investigations on Al-4wt% Cu alloys, which detail that due to age hardening, there is an improvement in their mechanical properties and the capacity to attain uniform phase dispersion through solid state methodology[16-19]. High-performance ceramics such as Al_2O_3, SiO_2, ZrO_2, SiC, TiC, B_4C, WC, ZrB_2, TiB_2, BN, AlN, SiN_4, fly ash and graphene are used as reinforcement material[20-22] to increase the strength of Al matrix. Adding ceramic particles in the Al matrix reduces stiffness; this can be resolved by decreasing the size of the ceramic particle to the nanometer scale[23]. Hybrid reinforcement applications utilize composite materials, including Al_2O_3-SiC[24], B_4C-SiC[25], B_4C-BN[26], Si-TiO_2[27], SiC-graphine[28] and have been processed into hybrid reinforcement materials.

This study uniquely examines the SiO_2-CrB_2 reinforcement in Al-Cu composites, a previously

*Corresponding author (E-mail: mvenkat@mech.sastra.edu)

investigated combination. Adding chromium boride improves the composite's mechanical, electrical, and corrosion resistance properties[29]. Reinforcement of 5% of SiO_2 in the Al matrix results in better modulus of elasticity, yield strength, and ultimate compression strength[30]. Nallusamy *et al.*[31] found that Al composite material having 4wt% % - 6wt% % of SiO_2 enhanced tensile strength, yield strength, and % of elongation. SiO_2 is synthesized by several methods, such as extraction from rice husk[32], sol-gel process[33], devitrification[34], etc. In these methods, Sol-Gel is the cost-effective method[35], having advantages such as large area deposition at atmospheric temperature, excellent homogeneity, accurate composition control, and the ability to coat curved surfaces.

This study reports the fabrication of lightweight metal matrix composites, reinforcing CrB_2 and synthesised SiO_2 in Al-Cu matrix alloy through compaction and sintering. Mechanical properties, including density, hardness, and compressive strength, are examined to determine the role of these reinforcing agents.

2 Materials and Methods

2.1 Synthesis of silica by sol-gel process

Initially, 12.5 ml of concentrated Hydrochloric Acid is dissolved in 35 ml of Deionized Water. The mixture is stirred with an electromagnetic stirrer with a hot plate at 350 RPM for 5 minutes at room temperature in the fume hood. The solution turns cloudy as HCl is added. 25 ml of TEOS is dissolved in 25 ml of absolute Ethanol. The mixture of TEOS and Ethanol is added to the latter solution at a constant temperature and stirring RPM. After 60 minutes of stirring, a cloudy solution is obtained, and the prepared sol is kept idle at room temperature for aging. The reaction occurring during the process is shown in equation (1).

$$Si(OC^2H^5)^4 + 4H^2O + HCl \rightarrow Si(OH)^4 + 4C^2H^5OH \rightarrow Si-O-Si + H^2O + C^2H^5OH \rightarrow SiO_2 + 2H_2O \quad \ldots (1)$$

After aging, the gel is dried at 120°C in the HTLP 45L hot air oven for 24 hours, forming silica crystals. The obtained crystals are ground with a pestle and mortar to get fine powders and then calcined at 700°C for 2 hours in the SA2-4-17TP box-type high-temperature furnace.

Elemental powders of high purity, namely Aluminum fine powder (98%), copper metal powder (99.99% – electrolytic grade), were purchased from LOBA CHEMIE, while chromium boride (99%) was purchased from Alfa Aesar. Finely ground SiO_2 powder synthesized by the sol-gel process was employed. Al with 4 wt% Cu was reinforced with 5 wt % SiO_2, 2.5 and 5 wt% CrB_2 and was homogenized using a motor mixer to achieve a homogeneous mixture.

Al_4Cu matrix alloy and Al_4Cu-based composites were cold compacted using a manual hydraulic press of a maximum capacity of 450 MPa. Green pellets of 10mm diameter and 15 mm thickness were obtained at the end of the process. Zinc stearate (10-15% ZnO) from Sisco Research Laboratories Pvt. Ltd was used as a lubricant to avoid internal friction in the die. The green pellets were sintered at a temperature of 550 °C at a heat rate of 10 ºC/min for 1.5 hours with a continuous Argon gas flow. The sintered samples were left for furnace cooling.

UV-vis and FTIR analyses were done on the sol-gel product to confirm the formation of SiO_2. X-ray diffractometer (XRD) was used for phase analysis. Archimedes method was employed to determine the densities of the sintered samples. Sintered samples were polished using SiC abrasive sheets (grades ranging from 400 to 2000 grit) and a disc polishing machine with alumina suspension, and etched with Keller's reagent (1.5 ml HCl, 2.5 ml HNO_3, 1 ml HF,

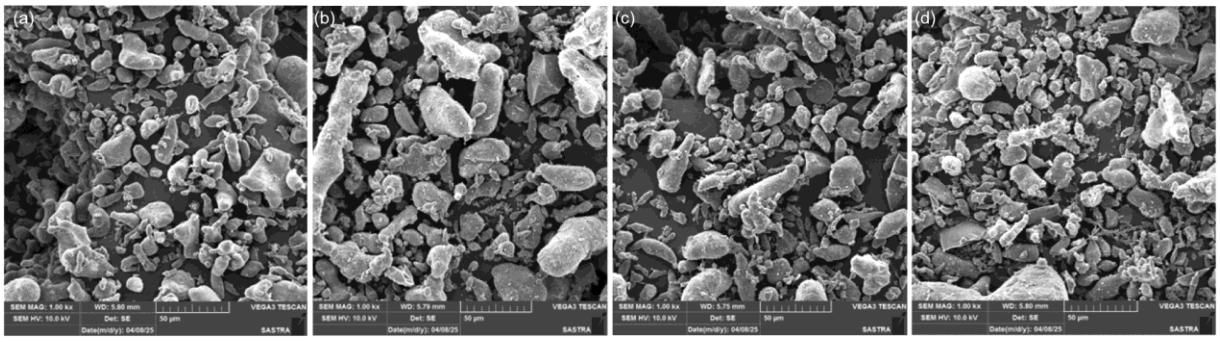

Fig. 1 — SEM image of (a) Al_4Cu, (b)$Al_4Cu_5SiO_2$, (c)$Al_4Cu_5SiO_2$ -2.5CrB_2 and (d)$Al_4Cu_5SiO_2$-5CrB_2 composite powders.

95 ml Distilled Water). An optical microscope was used to observe the microstructure of the samples. Hardness measurements were done by using Struers micro Vickers hardness tester (DuraVista-80) with a load of 25g and dwell time of 10 seconds. The compressive strength of Al alloy was assessed using a cylindrical sample (L/D ratio of 1.5) with a strain rate of 0.18mm/min. The nomenclature details are given in Table 1. The results and discussion are detailed in the next section.

3 Results and Discussion

3.1 Confirmation of silica

The confirmation of SiO_2 particles was carried out using Fourier Transform Infrared Spectroscopy (FTIR), by employing an Agilent Cary 630 FTIR spectrometer. This technique is widely utilized for identifying functional groups and bonding structures in materials due to its high sensitivity and specificity. The transmittance spectra were recorded in the 600–4000 cm^{-1} range to capture the characteristic vibrational modes associated with silica and related bonds.

For FTIR analysis, the silica sample was finely ground and homogeneously mixed with Aldrich potassium bromide (KBr - 99% pure), using a 2:98 sample-to-KBr ratio. The choice of KBr is necessary as it is IR-transparent and does not interfere with the spectral region of interest. Approximately 200 mg of the mixture was pressed into transparent pellets under high pressure to ensure uniform thickness and density, critical for minimizing scattering and enhancing spectral resolution. A background scan using pure KBr pellets was recorded before the sample measurement to eliminate ambient or material-related interferences.

As shown in Fig. 2, the FTIR transmittance spectrum shows a broad absorption band centered at 3462 cm^{-1}, corresponding to the O–H stretching vibrations associated with adsorbed moisture. The distinct peak observed at 1650 cm^{-1} denotes the stretching vibration of silanol (Si–OH) groups. These features indicate the hydrophilic nature of the synthesized silica surface.

Characteristic peaks identified at 1098 cm^{-1} and 795 cm^{-1}, confirms the presence of asymmetric and symmetric stretching vibrations of Si–O–Si bonds, respectively. These peaks are the most characteristic signatures of the siloxane (Si–O–Si) framework in silica. The spectral profile agrees with previously reported FTIR data for amorphous silica[33], confirming the successful synthesis of SiO_2 in the sample.

For further confirmation of the presence of Silica, UV-Visible spectroscopy was conducted using a HoverLabs UV-Vis spectrophotometer. The analysis was performed in the wavelength range of 190–1100 nm to assess the material's absorption behavior in the UV-VIS range.

Table 1 — Compositions and sample codes of the reinforcement mixtures.

Composition	Sample code
Al-4 wt% Cu	Al4Cu
Al-4 wt% Cu- 5 wt% SiO_2	Al4Cu5SiO_2
Al-4 wt% Cu-5 wt% SiO_2-2.5 wt % CrB_2	Al4Cu5SiO_2 -2.5CrB_2
Al- 4 wt% Cu- 5 wt% SiO_2-5 wt% CrB_2	Al4Cu5SiO_2-5CrB_2

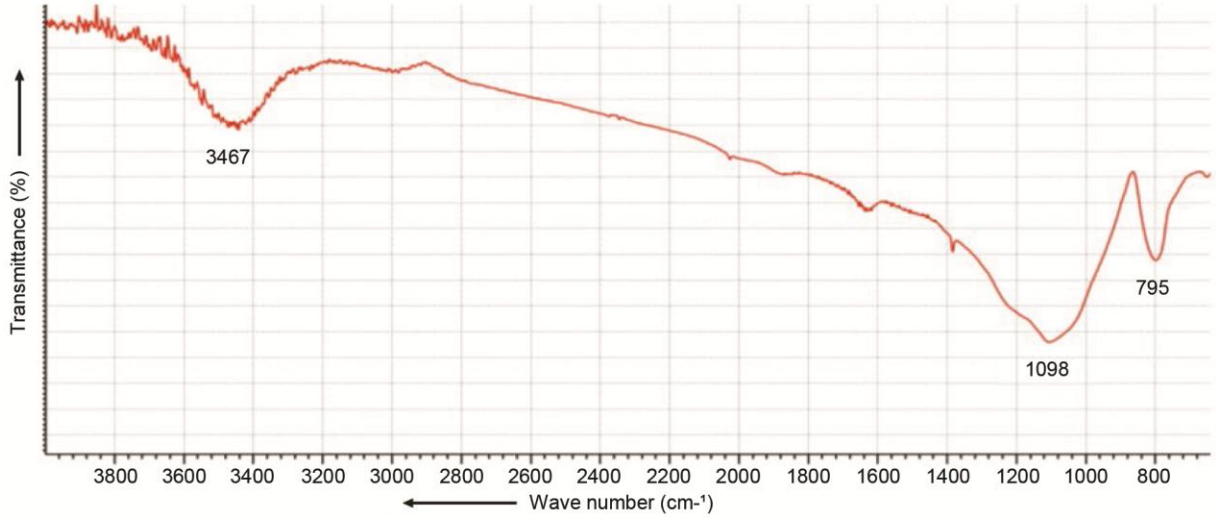

Fig. 2 — FTIR spectra of the synthesized silica sample by the sol-gel process.

E Péré *et al.*[36] found that the pure silica does not exhibit significant absorbance below 250 nm due to its wide band gap (approximately 8–9 eV), which prevents electronic excitation under UV-Vis radiation. Consistent with this, the obtained spectrum of the prepared silica showed minimal absorbance below 250 nm, as seen in Fig. 3. Also, there is a gradual and continuous decline in absorbance with increasing wavelength. The absence of sharp absorption peaks indicates a lack of chromophoric impurities or defects within the silica matrix[33].

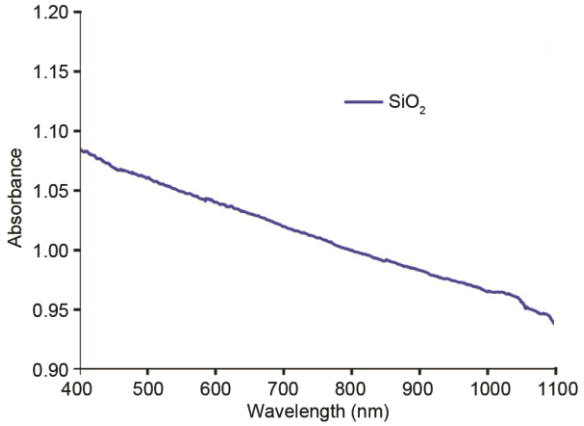

Fig. 3 — UV vis absorption spectrum of synthesized silica particles.

These spectroscopic analyses confirm the successful formation of high-purity silica with well-defined structural and optical characteristics.

The microstructural image of the Al4Cu composite has a fine grain structure, which is depicted in Fig. 4(a). A few dark, irregularly shaped spots distributed in the matrix are observed, which are likely the ceramic particles introduced into the composite. These dark regions increase as the percentage of ceramic particles increases, as shown in Fig. 4(b-d). The formation of the intermetallic phases and the presence of ceramic particles have been additionally validated by X-ray Diffraction (XRD) analysis.

The XRD patterns of Al4Cu and its composites are shown in Fig. 5, which demonstrates that only the peaks of Al and Al_2Cu phase are formed in all the sintered samples[29]. This proves that no intermediate phase formation occurred during the sintering process. Ganesh *et al.*[37] stated that the formation of intermetallic Al2Cu occurs at 548 °C due to the interaction between Al and Cu. Aravind *et al.*[38] observed the higher peaks of Al and Al_2Cu during sintering. The XRD results show that the synthesized silica is amorphous; therefore, no distinguishable peaks were observed[39]. The XRD pattern for the CrB_2

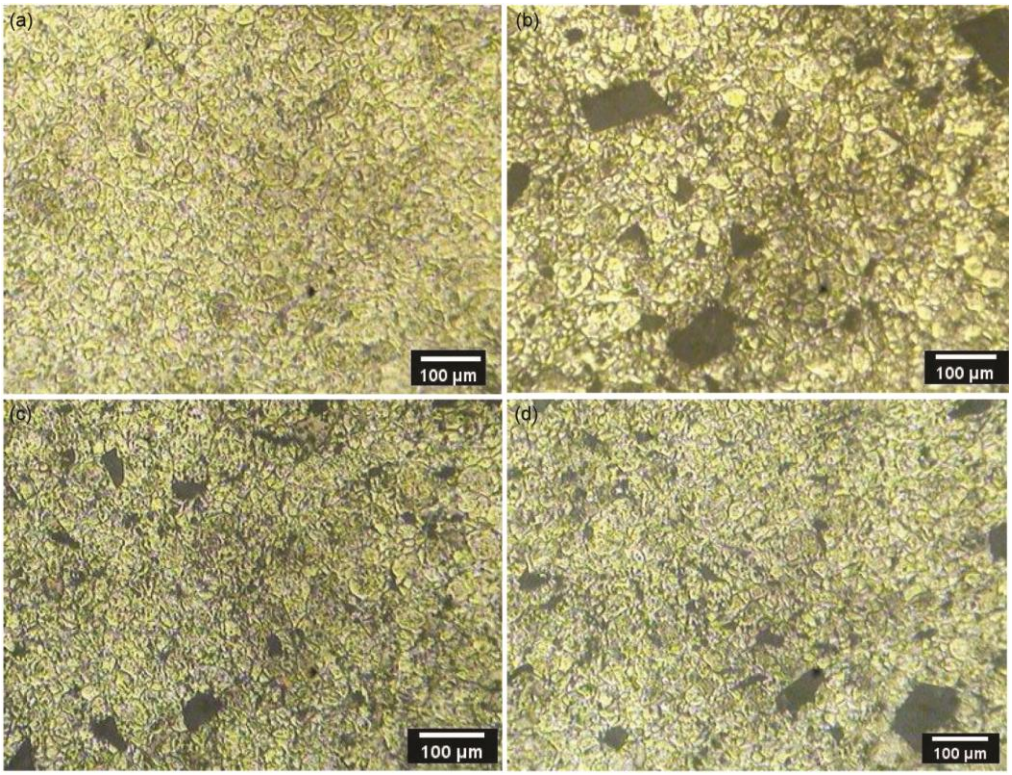

Fig. 4 — Microstructure of (a) Al_4Cu, (b) $Al_4Cu_5SiO_2$, (c) $Al_4Cu_5SiO_2$ -2.5CrB_2 and (d) $Al_4Cu_5SiO_2$-5CrB_2

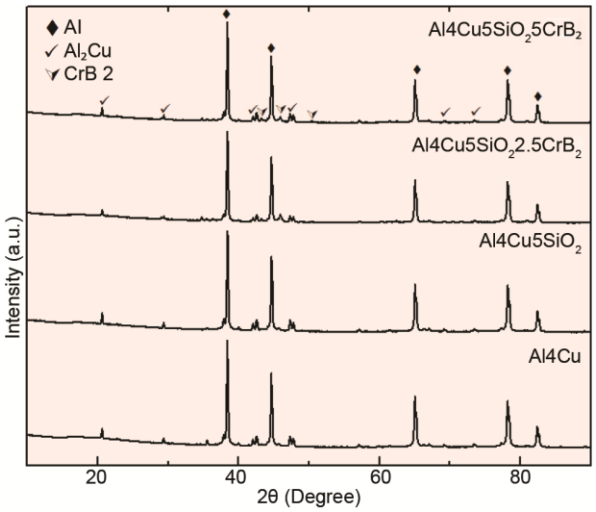

Fig. 5 — XRD patterns of the sintered composites.

Table 2 —Density of the sintered composites.

Sample	Theoretical Density (g/cc)	Archimedes Density (g/cc)	Relative Density (%)
Al4Cu	2.78	2.47	88.84
$Al4Cu5SiO_2$	2.77	2.46	88.87
$Al4Cu5SiO_2$ - $2.5CrB_2$	2.81	2.59	92.1
$Al4Cu5SiO_2$-$5CrB_2$	2.84	2.36	83.09

peaks agrees with the previous investigation[40]. From the study, it can be concluded that neither the silica nor the chromium boride particles decomposed to any other form or phase during the sintering process.

The theoretical densities of Al4Cu and reinforced Al4Cu matrix were calculated by the rule of mixtures. The Relative density and Archimedes density are mentioned in Table 2. The density increases as the wt% of reinforcement increases because Cu (8.94 g/cc) and CrB_2 (5.15 g/cc) have high densities. The relative densities of sintered samples range between 83.09% to 92.1%. Leszczynska *et al.*[41] found that Al-4wt% Cu after compaction and sintering had a relative density of 89%. Relative densities of Al-4wt% Cu range between 81% to 91% and were reported in a study by Wolla *et al.*[42] The formation of intermetallic precipitates such as Al_2Cu, Al_9Cu_4, reduced densification produced by SPS, and was investigated by Kim *et al.* From the previous studies, Al+4wt% Cu had a relative density of 89% which is quite similar to the result obtained[43]. This is due to the presence of intermetallic precipitate Al_2Cu (has a density of about 4.4 g/cc).

Hard and brittle particles reinforced in a ductile metal matrix reduce the diffusion between the metal

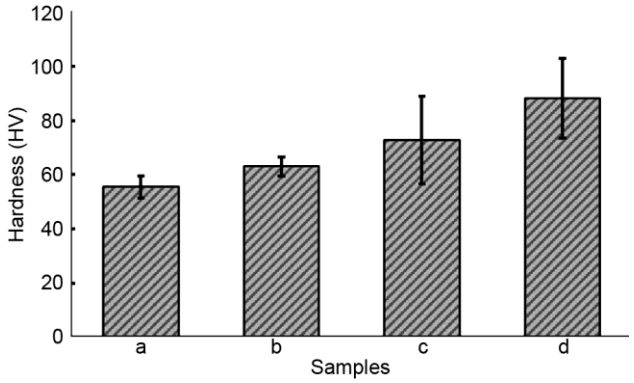

Fig. 6 — Hardness values of (a)Al_4Cu, (b) $Al_4Cu_5SiO_2$, (c) $Al_4Cu_5SiO_2$ -$2.5CrB_2$ and (d) $Al_4Cu_5SiO_2$-$5CrB_2$ sintered composites.

particles during sintering[44-46]. This is because low diffusion densification is diminished. $Al4CuSiO_2$-$2.5CrB_2$ had the highest density of 92.1% when compared to Al4Cu. There is a 3.6% increase in relative density. An increase of 2.5 % of CrB2 reduces 10% relative density. This denotes that increasing the wt% of CrB_2 above 2.5% in the $Al4Cu5SiO_2$ matrix reduces the densification.

Post-sintering, the development and dispersion of the Al_2Cu intermetallic phase serve to substantially bolster the hardness of Al–Cu alloys[38,47,43]. In related studies, sintering has consistently resulted in the emergence of intermetallic Al_2Cu precipitate, resulting in increased hardness across all sintered samples. The hardness value of Al4Cu is 55.5HV in Fig. 6, which is much closer to 52.02HV obtained by Ganesh *et al.*[37]. The hardness value gradually increases as the reinforcement wt.% is increased. The inter-particle distance decreases as the amount of reinforcement in the Al alloy matrix increases. The closer spacing of the materials restricts the movement of dislocations, consequently enhancing the structural rigidity of the composite [29]. The hardness of silica and Chromium boride is found in the range of 550.6-652.6 HV and 1631HV, respectively[49-50]. Adding 5 wt% silica and chromium boride in the Al4Cu alloy matrix increases the hardness from 55.5 HV to 95 HV. Though no interfacial bonding is created between the reinforcement and matrix, it restricts the motion of the dislocation during indentation. Adding 5 wt% silica aluminum composite increases the hardness value, but only by 16.5%, whereas adding 5% Silica and 5% CrB2 increases the hardness value by 52%.

Figure 7 presents the compression test results of Al4Cu alloy and SiO_2, CrB_2 reinforced composites. Al4Cu and $Al4Cu5SiO_2$ matrices have the highest

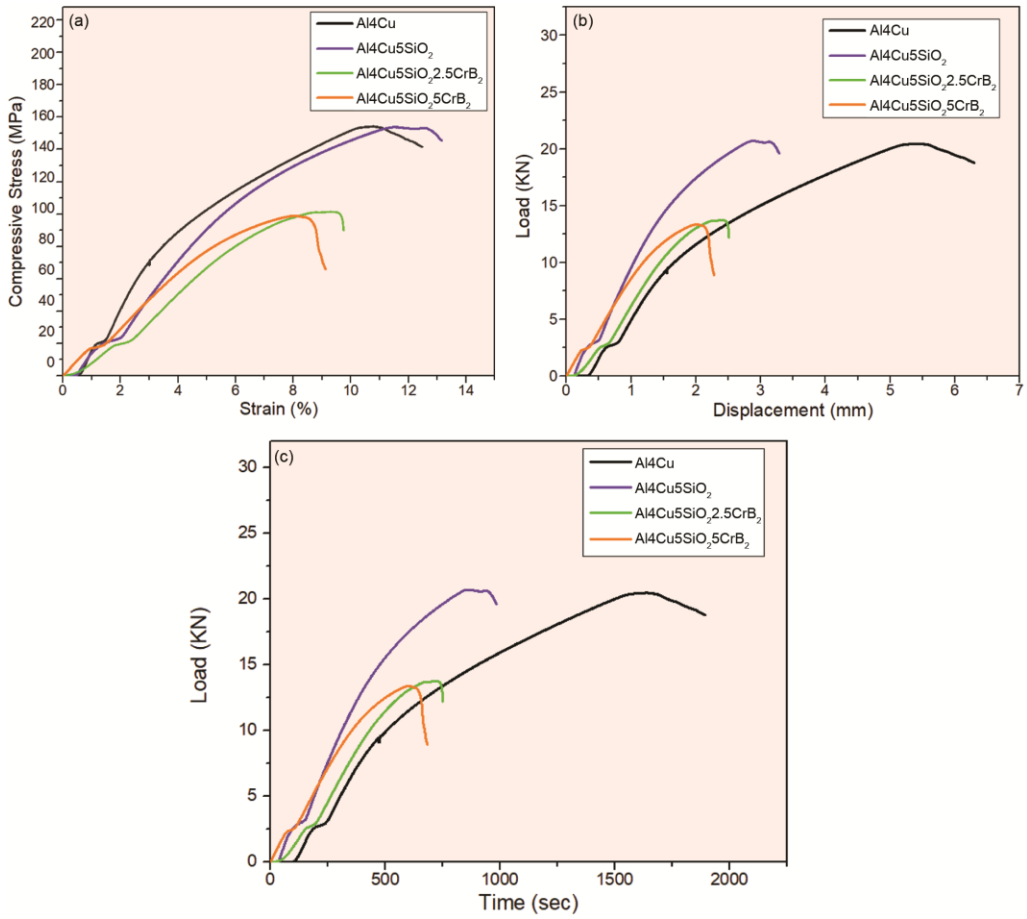

Fig. 7 — (a) Compressive stress-strain, (b) Load-displacement and (c) Load-time curves of the Al_4Cu alloy and SiO_2 and CrB_2 reinforced composites.

compressive strength of 151 MPa. Adding 2.5wt% and 5wt% in the Al4Cu5SiO_2 matrix reduces the compressive strength to 101 MPa and 99 MPa. An increase in reinforcement wt% results in increased hardness, but is not directly proportional to the compressive strength. Clustering of composite particles can occur after adding a critical wt% of reinforcement[45]. It was also observed that samples prepared from ball-milled powders have higher compressive strength than samples fabricated with unball-milled powder[51]. Mechanical alloying helps to disperse the reinforcement into the matrix properly. Compressive strength is affected because of inhomogeneously located reinforcement clusters that lead to crack formation[45] and cause the sample to fail early (Fig. 7(c)). The highest displacement was found in the Al4Cu matrix alloy (Fig. 7 (b)), which denotes it has plastically deformed more than the other composite samples. The addition of SiO_2 and CrB_2 reduced the alloy's ability to deform because of restrictions on dislocation plastically.

4 Conclusion

This research paper investigates the effect of reinforcement of amorphous silica synthesized by the sol-gel method and CrB_2 in Al4Cu. The powders were mixed, cold compacted, and sintered. Based on the results, the following conclusion can be drawn.

a The peaks at 1098 cm^{-1} and 795 cm^{-1} in FTIR analysis confirm the formation of Si-O-Si bonds in the synthesized silica. Additional confirmation was done using UV Vis spectroscopy, where the silica had absorption below 250 nm

b Successive additions of reinforcement particles lead to a progressive rise in the hardness values. Composite reinforced with 5% of SiO_2 and CrB_2 has the maximum hardness of 95HV.

c The highest compressive strength of 151 MPa was observed in Al4Cu and Al4Cu5SiO2 matrices. Further addition of chromium boride leads to a progressive reduction of the compressive strength. This was an inverse trend compared to several studies that have reported

compressive strength increases with the addition of SiO_2 and CrB_2 in the metal matrix. Non-uniform distribution of ceramic particles is attributed to weak interfacial bonding at the matrix-reinforcement interface, which introduces stress concentrators. Optimizing the powder mixing procedure could address these limitations in future studies.

d X-ray diffraction analysis confirm the presence of Al_2Cu after sintering at 550 °C and the presence of CrB_2. The highest relative density of 92.1% was found in Al4Cu5SiO2-2.5CrB2.

Acknowledgment

The authors would like to sincerely thank N-ERGY AI SOLUTIONS INDIA PRIVATE LIMITED for providing the experimental facilities.

References

1 Garg P, Jamwal A, Kumar D, Sadasivuni K K, Hussain C M & Gupta P, J Mater Res Technol, 8 (2019) 4924.
2 Tekoğlu E, Ağaoğulları D, Mertdinç S &Öveçoğlu M L, J Mater Sci, 53 (2018) 2537.
3 Alem S A A, Latifi R, Angizi S, Hassanaghaei F, Aghaahmadi M, Ghasali E &Rajabi M, Mater Manuf Process, 35 (2020) 303.
4 Kaftelen H, Ünlü N, Goller G, Öveçoğlu M L & Henein H, Compos Part A ApplSciManuf, 42 (2011) 812.
5 Dong X, Youssef H, Zhang Y, Wang S & Ji S, Compos Part B Eng, 177 (2019) 107453.
6 Miracle D B, Compos SciTechnol, 65 (2005) 2526.
7 Bhoi N K, Singh H & Pratap S, J Compos Mater, 54 (2020) 813.
8 Ganesh V, Hemsainad P &Khanra A K, J Mater Sci, 59 (2024) 17394.
9 Sharma S K, Gajević S, Sharma L K, Pradhan R, Sharma Y, Miletić I &Stojanović B, Lubricants, 12 (2024) 421.
10 Singh A K, Soni S & Rana R S, AdvEng Mater, 22 (2020) 2000322.
11 Yan J, Xu Z, Shi L, Ma X & Yang S, Mater Des, 32 (2011) 343.
12 Uzun H, Mater Des, 28 (2007) 1440.
13 Ingarao G & Priarone P C, J Manuf Process, 56 (2020) 1219.
14 Thavasilingam K, Sakthimurugan D & Giridharan K, Aerospace Materials, (2025) 385.
15 Yang C, Zhang P, Shao D, Wang R H, Cao L F, Zhang J Y, Liu G, Chen B A & Sun J, Acta Mater, 119 (2016) 68.
16 Wang S C &Starink M J, Int Mater Rev, 50 (2005) 193.
17 Hamzah A H, Al-Khafaji H M H & Hussein T S, Int J Heat Technol, 42 (2024) 297.
18 Prados E F, Sordi V L & Ferrante M, Acta Mater, 61 (2013) 115.
19 Meng X, Liu T, Shi C, Liu E, He C & Zhao N, Mater Sci Eng A, 633 (2015) 103.
20 Taha M A, Nassar A H &Zawrah M F, Constr Build Mater, 248 (2020) 118638.
21 Bian Y, Gao T, Liu L, Liu G & Liu X, J Alloys Compd, 842 (2020) 155926.
22 Anand V K, Aherwar A, Mia M, Elfakir O & Wang L, TribolInt, 151 (2020) 106514.
23 Teng X, Liu H & Huang C, Mater Sci Eng A, 452 (2007) 545.
24 Halil K, İsmail O, Sibel D & Ramazan Ç, J Mater Res Technol, 8 (2019) 5348.
25 Uthayakumar M, Aravindan S &Rajkumar K, Mater Des, 47 (2013) 456.
26 Chand S & Chandrasekhar P, Ceram Int, 46 (2020) 17621.
27 Sharma R &Baral J, J Mater Eng Perform, 34 (2025) 5212.
28 Reddy K S K, Kannan M, Karthikeyan R, Sripad A & Jain P K, Mater Today Proc, 26 (2020) 2746.
29 Mertdinç S, Kılık M, Baltaş Ş, Taşkın A K, Öveçoğlu M L & Ağaoğulları D, Solid State Sci, 120 (2021) 106727.
30 Munasir, Triwikantoro, Mochamad Z, Bäßler R & Darminto, J Phys Sci, 30 (2019) 81.
31 Nallusamy S &Logeshwaran J, J Metastable Nanocryst Mater, 29 (2017) 25.
32 Bakar R A, Yahya R & Gan S N, Procedia Chem, 19 (2016) 189.
33 Dubey R S & Rajesh Y B R D M A, Mater Today Proc, 2 (2015) 3575.
34 Zhu Y, Pan Y, Xu H &Guo J, J Non-Cryst Solids, 355 (2009) 785.
35 Vishwas M, Rao K N, Phani A R, Gowda K A & Chakradhar R P S, Spectrochim Acta A Mol Biomol Spectrosc, 78 (2011) 695.
36 Péré E, Cardy H, Cairon O, Simon M & Lacombe S, VibSpectrosc, 25 (2001) 163.
37 Ganesh V, Tamboli R R, Khanra A K &Dey S R, Vacuum, 225 (2024) 113251.
38 Aravind M, Yu P, Yau M Y & Ng D H, Mater SciEng A, 380 (2004) 384.
39 Zainuri M &Bäßler R, J Phys Sci, 30 (2019) 81.
40 Gudyma T S, Shestakov V A, Dik D V, Krutskii Y L, Anisimov A G, Cherkasova N Y & Ukhina A V, Nanobiotechnol Rep, 18 (2023) 55.
41 Tylek A, Leszczyńska-Madej B & Zygiert A, Key Eng Mater, 682 (2016) 252.
42 Wolla D W, Davidson M J & Khanra A K, Int J Mech Mater Eng, 10 (2015) 8.
43 Kim K, Kim D, Park K, Cho M, Cho S & Kwon H, Materials, 12 (2019) 1546.
44 Ağaoğulları D, Ceram Int, 45 (2019) 13257.
45 Tekoğlu E, Ağaoğulları D, Mertdinç S, Paksoy A H & Öveçoğlu M L, Adv Powder Technol, 29 (2018) 2070.
46 Rahimian M, Ehsani N, Parvin N & Baharvandi H R, Mater Des, 30 (2009) 3333.
47 Azizieh M, Dezfuli M A G, Balak Z & Kim H S, Mater Res Express, 6 (2019) 036528.
48 Mehditabar A, Rahimi G H & Vahdat S E, Sci Eng Compos Mater, 26 (2019) 327.
49 Wang S, Yu X, Zhang J, Zhang Y, Wang L, Leinenweber K, Xu H, Popov D, Park C, Yang W & He D, J Superhard Mater, 36 (2014) 279.
50 Cairns D R, Kessman A J, Richter P J, Bottari F J & Randall N X, Wear, 265 (2008) 411.
51 Das D K, Mishra P C, Singh S & Ratish K T, Int J Mech Mater Eng, 9 (2014) 12.